A New Design Optimization Method for Permanent Magnet Synchronous Linear Motors

Authors:

Juncai Song, Fei Dong, Jiwen Zhao, Siliang Lu, Le Li, Zhenbao Pan

Date Submitted: 2019-02-27

Keywords: gravity center neighborhood algorithm (GCNA), non-parametric quick calculation model, multiple support vector machine (multi-SVM), 3D finite element analysis (3D-FEA), thrust ripple, thrust, permanent magnet linear synchronous motors (PMSLM)

Abstract:

This study focused on the design optimization of permanent magnet synchronous linear motors (PMSLM) that are applied in microsecond laser cutting machines. A new design optimization method was introduced to enhance PMSLM performances in terms of motor thrust, thrust ripple, and inductive electromotive force (EMF). Based on accurate 3D finite element analysis (3D-FEA), a multiple support vector machine (multi-SVM) was proposed to build a non-parametric quick calculation model by mapping the relation between multivariate structure parameters and multivariate operation performances. The gravity center neighborhood algorithm (GCNA) was also applied to search the global optimal combination of the structure parameters by locating the gravity center of the multi-SVM model. The superiority and validity of this method are verified by experiments.

Record Type: Published Article

Submitted To: LAPSE (Living Archive for Process Systems Engineering)

Citation (overall record, always the latest version): LAPSE:2019.0303
Citation (this specific file, latest version): LAPSE:2019.0303-1
Citation (this specific file, this version): LAPSE:2019.0303-1v1

DOI of Published Version: https://doi.org/10.3390/en9120992

energies

MDPI

Article

A New Design Optimization Method for Permanent Magnet Synchronous Linear Motors

Juncai Song, Fei Dong, Jiwen Zhao *, Siliang Lu, Le Li and Zhenbao Pan

College of Electrical Engineering and Automation, Anhui University, Hefei 230601, China; songjuncai528@gmail.com (J.S.); feidong@ahu.edu.cn (F.D.); silianglu@ahu.edu.cn (S.L.); lile15755145309@outlook.com (L.L.); pzhenbao@gmail.com (Z.P.)

* Correspondence: ustczjw@ahu.edu.cn; Tel.: +86-138-5517-6449

Academic Editor: Chunhua Liu

Received: 28 July 2016; Accepted: 18 November 2016; Published: 25 November 2016

Abstract: This study focused on the design optimization of permanent magnet synchronous linear motors (PMSLM) that are applied in microsecond laser cutting machines. A new design optimization method was introduced to enhance PMSLM performances in terms of motor thrust, thrust ripple, and inductive electromotive force (EMF). Based on accurate 3D finite element analysis (3D-FEA), a multiple support vector machine (multi-SVM) was proposed to build a non-parametric quick calculation model by mapping the relation between multivariate structure parameters and multivariate operation performances. The gravity center neighborhood algorithm (GCNA) was also applied to search the global optimal combination of the structure parameters by locating the gravity center of the multi-SVM model. The superiority and validity of this method are verified by experiments.

Keywords: permanent magnet linear synchronous motors (PMSLM); thrust; thrust ripple; 3D finite element analysis (3D-FEA); multiple support vector machine (multi-SVM); non-parametric quick calculation model; gravity center neighborhood algorithm (GCNA)

1. Introduction

Permanent magnet synchronous linear motors (PMSLM) are widely used in high-precision microsecond laser cutting machines. Compared with the conventional solution-routing motors with ball screws, PMSLM has absolute predominance in terms of high acceleration, excellent accuracy, and direct drive [1]. The quantity of manufactured products is guaranteed by the remarkable operational performances of PMSLM.

High acceleration and efficiency are significant to the operating quality of PMSLM. Thrust is one of the most important indices of PMSLM performance that can influence the acceleration of the mover, which is similar to torque in rotatory motors. Thrust ripple is becoming the largest problem that can result in a decreased accuracy of the mover position [2]; it is the fluctuation of stable thrust that can lead to scratching on the surface of products, increase roughness, and produce dimension errors. The main influencing elements of the thrust ripple are the structure parameters, control method, and load; all of the elements are gathered together nonlinearly. Two main schemes for the suppression of the thrust ripple are the design optimization of PMSLM and advanced control strategies, with the former being the dominant method [3].

The design optimization of PMSLM is a multi-objective problem due to the great number of design parameters, objectives, and constraints [4]. The most important issues in the design optimization are models and algorithms. Firstly, the commonly used optimization models include the analytic model [5,6], the finite-element model (FEM), the approximate models [7–9], but it is very difficult to apply the abovementioned optimization models due to the nonlinear and high dimensionality of PMSLM

optimization. The major shortcoming of the analytic model and approximate model is the accuracy problem: given the essential assumptions, and the veracity of the objective functions, these models based on the equivalent magnetic circuit will result in an accuracy decrease [10]. The FEM model is accurate, but it has low efficiency, which requires a significant computing cost. Another modified method based on the FEM model are robust design optimization methods [11,12], which are generally employed for high-quality designs, including product robustness against noise factors in manufacturing and operational environments. The most representative are six-sigma [13,14] and Taguchi methods [15–18] which use mathematical statistics and design of experiments, methods that can promote the efficiency of FEM models by using an orthogonal array, they are widely used in industry applications' optimization. However, the shortcoming of these methods is that only analyzing discrete sample space based on different combinations of motor structure parameters may result in an approximate local optimum for the motor optimization design. Another important issue is in the design optimization algorithms. Nowadays, many modern intelligent optimization algorithms, such as genetic algorithms (GA) [7] and particle swarm optimization algorithms [19], are becoming very popular as they can handle problems with strong nonlinearity, but the global search ability and rapidity need to be enhanced.

All of the above-mentioned methods are inappropriate in terms of accuracy and reliability in PMSLM design optimization. This present study proposes a new design optimization method for PMSLM. First, a 3D-FEA model is built to obtain the accurate operation performances of PMSLM and the sample data space based on different structural parameters. Second, a multiple support vector machine (multi-SVM) is introduced to map the relation between the space of the multivariate structure parameters and the multivariate operational performance. It is a new machine learning method for regression which have been effectively applied in function estimation [20], fault diagnosis [21], and data mining [22]. In this study, the space of the discrete data based on 3D-FEA is translated into a continuous data space by multi-SVM regression, which can provide a non-parametric quick calculation model for follow-up optimization. Finally, the gravity center neighborhood algorithm (GCNA) [23] is presented, and the "filling function" [24] is introduced to avoid the premature convergence and local optimal of GCNA. The global optimal combination of the structure parameters is realized upon the convergence of the iteration. The superiority and validity of this method are confirmed by the 3D-FEA and experimental test.

The paper is organized as follows: Section 2 introduces the characteristics of PMSLM; Section 3 introduces the used Taguchi optimization method; Section 4 proposes the new design optimization method for PMSLM; Section 5 verifies and discusses the superiority and practicability of the proposed method by experimental results; Section 6 draws the conclusions; and Section 7 discusses future work.

2. Characteristic Presentation

The initial design model of the PMLSM is shown in Figure 1. The main mechanical structure of this PMSLM was made of back-iron, coils and magnets. This motor has three-phase, seven-pole, six-coils (A, X, B, Y, C, and Z), and a double secondary. The machine design structure is the "U"-model structure. The number of coils is six, and three phases are "Y" connected.

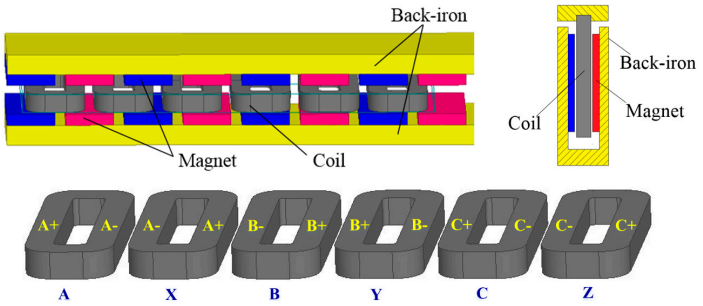

Figure 1. Permanent magnet synchronous linear motors (PMSLM) with a double secondary.

The layer analysis model of the PMSLM is shown in Figure 2, and there are three regions: region I are the coils, region II are the permanent magnets, and region III is the back-iron. This PMSLM design implies the considerations of six main variable structural parameters: the magnet length (τ_m), the magnet height (h), the air gap between magnets and coils (δ), the pole pitch (τ), the coil length (l), and the coil width (d). Aside from these, the materials of the PM and back-iron should also be considered. The PMs consist of NdFe material with a remanence (B_r) of 1.43 T, and the stator consists of M20 steel silicon. The magnet length, magnet width, and coil width are fixed at 40, 15, and 40 mm, and the turns per coil are 180. Given that the other parameters are regarded as fixed and known, different combinations of structure parameters can result in different output performances of PMSLM. The best performance are determined via the global optimization of the motor structure.

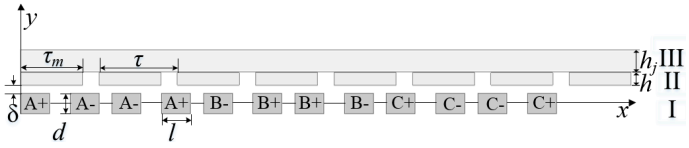

Figure 2. Layer analysis model of the PMSLM.

3. Taguchi Optimization Method

The Taguchi method is a multi-objective optimization method using the analysis of means (ANOM) [10,15–18]. Figure 3 shows the comprehensive framework of the Taguchi method: the first step is building the FEM model of PMSLM and analyzing the performances data, followed by applying the Taguchi optimization method, which includes design of experiments (DOE) and ANOM. Finally, according to the different sensitivities of the different factors, select the best combination of motor structure parameters. All of these are shown as follows.

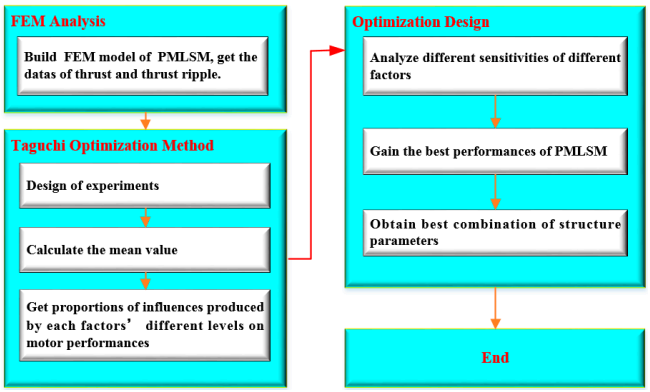

Figure 3. Framework of Taguchi optimization method.

3.1. Establishment of Orthogonal Array

A finite-element parametric model of a PMSLM was built. After the FEM mesh generation, shown in Figure 4, all of the performances of the motor in the matrix experiments were analytically demonstrated in [25].

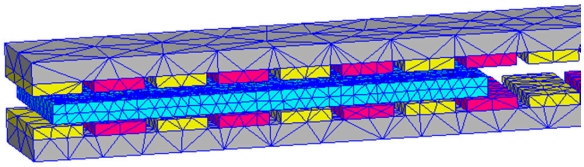

Figure 4. 3D-FEM model of a PMSLM.

According to design principles of PMSLM four parameters, including height of magnets (h), air gap (δ), pole pitch (τ), and coil length (l), were selected as variable parameters. In Table 1, the value range of h is from 2.0 to 3.5 mm, δ is from 1.6 to 2.2 mm, τ is from 17 to 20 mm, and l is from 6.0 to 7.5 mm. All of the value ranges are generally satisfied with the requirements of microsecond laser cutting machines, namely, thrust should be no less than 35 N, and thrust ripple and harmonic contents should be the lowest.

Table 1. Four main structural variables of the motor.

No.	Parameters	Description	Value Range
1	h	height of magnets	2.0–3.5 mm
2	δ	air gap	1.6–2.2 mm
3	τ	pole pitch	17–20 mm
4	l	coil length	6.0–7.5 mm

The Taguchi method is known as the design of experiments using an orthogonal array to screen the experimental conditions and means [26]. In Table 2, three levels of four undetermined factors: h, δ, τ, and l were shown clearly as the level step of each factor is 0.75 mm, 0.3 mm, 1.5 mm, and 0.75 mm, respectively. As shown in Table 3, a Taguchi orthogonal array L_9 (3^4) is then established for numerical experiments. In this Table, the nine-group FEA simulation experiments were conducted, all of the motor's performances, such as F (average thrust), η (thrust ripple), and THD (harmonic distortion rate), were analyzed.

Table 2. Levels of the main factor variables.

Factor Variables	Level 1	Level 2	Level 3
A: h (mm)	2.0	2.75	3.5
B: δ (mm)	1.6	1.9	2.2
C: τ (mm)	17	18.5	20
D: l (mm)	6.0	6.75	7.5

Table 3. Experimental arrays and results of finite element analysis (FEA).

No.	Levels of Each Factor				Performances		
	A	B	C	D	F (N)	η (%)	THD(%)
1	2.0	1.6	17	6.0	36.084	10.804	5.214
2	2.0	1.9	18.5	6.75	34.143	10.796	5.517
3	2.0	2.2	20	7.5	31.102	12.273	6.425
4	2.75	1.6	18.5	6.75	40.797	10.542	3.333
5	2.75	1.9	20	6.0	37.514	8.342	2.243
6	2.75	2.2	17	7.5	38.168	9.973	2.155
7	3.5	1.6	20	6.75	45.109	9.135	2.067
8	3.5	1.9	17	7.5	43.083	10.161	6.031
9	3.5	2.2	18.5	6.0	40.315	12.897	4.153

3.2. Analysis of Mean Value

The Taguchi optimization method uses the statistical mean made by orthogonal arrays and analysis results of FEA. The average values of each motor performance (F, η, and THD) are shown in Table 4:

Table 4. Average values of each performance.

Performances	F (N)	η (%)	THD (%)
Average Values	38.479	10.547	4.126

The average value of different performances at different levels are calculated using Equation (1):

$$G_{xi}(P_x) = \frac{1}{3}[P_x(l_1) + P_x(l_2) + P_x(l_3)] \quad (1)$$

x represents the different factors: A, B, C, D; i represents the levels of factors: 1, 2, 3; P_x represents the motor performances: F (N), η (%), THD (%); $Gx_i(P_x)$ represents the average values of performances under x factor at i level; and $P_x(l_i)$ represents the values of performances under x factor at i level as shown in Table 3.

For example, the average value of F under factor $C(\tau)$ at level 3 is calculated as Equation (2):

$$\begin{aligned} G_{C3}(F) &= \tfrac{1}{3}[F(3) + F(5) + F(7)] \\ &= \tfrac{1}{3}[31.102 + 37.514 + 45.109] = 37.908 \end{aligned} \quad (2)$$

All of the average values of performances under each level of factor variable index are obtained as shown in Table 5.

Table 5. Average values of performance under each level of factor variable index.

Variables	Level of Each Factor	F (N)	η (%)	THD (%)
A	1	33.776	11.291	5.179
	2	38.826	9.619	2.577
	3	42.836	10.731	4.084
B	1	40.663	10.160	3.538
	2	38.247	9.766	4.597
	3	36.528	11.714	4.244
C	1	39.112	10.313	4.467
	2	38.418	11.412	4.334
	3	37.908	9.917	3.578
D	1	37.971	10.681	3.870
	2	40.016	10.158	3.639
	3	37.451	10.802	4.870

According to Table 5, the influence of each factor on F, η, and THD are as shown in Figure 5. It is noted in Figure 5 that, combination (A3, B1, C1, and D2) contribute to the maximization of F, combinations (A2, B2, C3, and D2) contribute to the minimization of η, combination (A2, B1, C3, and D2) contribute to the minimization of THD. However, no elements are obviously selected to constitute the combination of the optimum design for maximum F, minimum η, and THD at the same time.

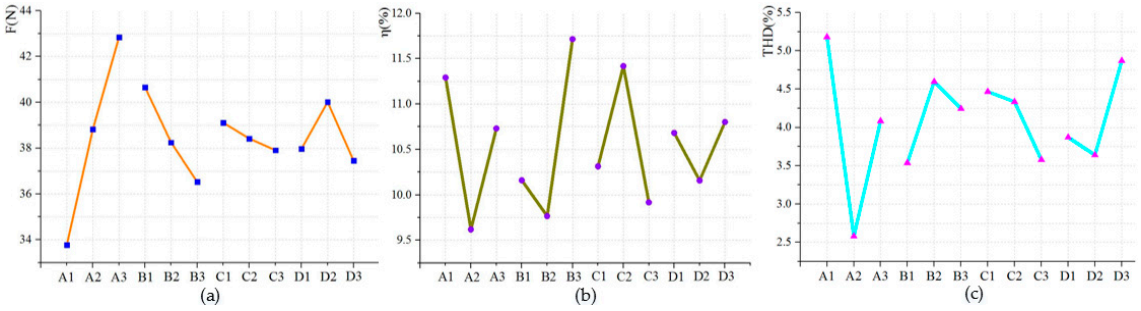

Figure 5. Main factor effects on motor performances: (**a**) F (N); (**b**) η (%); and (**c**) THD (%).

3.3. Proportions of Influences Produced by Each Factor's Different Levels on Motor Performances

The sum of error squares (SS) is a measure of the deviation of the experimental data from the average value of data, SS generated by various factors and different levels can be calculated as Equation (3). All of the results of SS and proportion are reported in Table 6.

$$SS = 3\sum_{i=1}^{3}\sum_{j=1}^{3}[M_{x_i}(P_{x_i}) - M(P_j)]^2 \quad (3)$$

x represents the different factors: A, B, C, D; i represents the levels of factors: 1, 2, 3; P represents the motor performances: F (N), η (%), THD (%); $Mx_i(Px_i)$ represents the average values of performances under x factor at i level as shown in Table 5; and $M(P_j)$ represents the average values of performance as shown in Table 4.

Table 6. Proportion of influences produced by various factors on motor performance.

Various Factors	*F*		*η*		THD	
	SS	Proportion (%)	*SS*	Proportion (%)	*SS*	Proportion (%)
A	123.67	76.0	4.35	29.0	10.53	64.9
B	25.89	15.9	6.36	42.3	1.74	10.7
C	2.19	1.3	3.60	24.0	1.38	8.6
D	11.03	6.8	0.70	4.7	2.57	15.8
Total	162.78	100	15.01	100	16.22	100

As shown in Table 6: (1) F is most sensitive to A, as B has a relatively weak effect on F; (2) η is sensitive to A, B, and C, B is the most sensitive factor as A, C have nearly a similar effect on η; (3) THD is most effected by A, as D has a moderate effect. To achieve this multiple-optimization goal, according to Figure 5 and Table 6, the best combination of factors is selected to be (A2, B2, C3, and D2). In conclusion, the PMSLM performances based on the Taguchi method are: F is 40.241 N, η is 6.342%, and the THD is 2.66%.

4. Proposed New Optimization Method

In Section 3, the Taguchi method was conducted, which had some effect on PMSLM optimization. The optimization results are F is 40.241 N, η is 6.342%, and the THD is 2.66%. However, it had one relatively serious shortcoming: in the optimization process, the four parameters and three levels can result in 3^4 = 81 combinations. This method based on FEA analysis, in which only nine groups of parameter combinations are analyzed, can promote the efficiency by using ANOM. However, given the one-sidedness produced by the discrete sample space of FEA, this method can only obtain the best optimization results from 81 discrete combinations, not from the global optimum of the parameter continuous value range. This method results in an approximate local optimum for the motor optimization design.

This study proposes a new design optimization method to overcome the shortcomings of the Taguchi method. A flowchart of this method is shown in Figure 6.

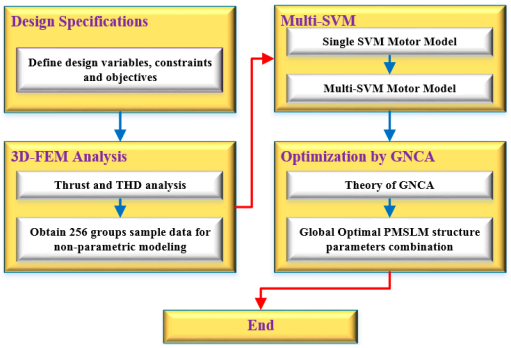

Figure 6. Flowchart of the proposed optimization method.

In this method, the 3D-FEA model is developed to obtain the accurate motor output performances after the definition of the design variables, constraints, and objectives. A total of 256 combinations of

the structure parameters are analyzed by 3D-FEA to prepare for the following multi-SVM modeling. Multi-SVM is then introduced to build a quick non-parametric calculation model based on 3D-FEA analysis data. After regression, the multi-SVM motor model translates the discrete motor data space into continuous data space, which can avoid local one-sided optimization. Finally, the gravity center neighborhood algorithm (GCNA) is presented to optimize the multi-SVM motor model by locating the gravity center of the objective function. The global optimal combination of the structure parameters is obtained upon convergence of the iteration.

4.1. 3D-FEA for Modeling Data Gaining

The value range of four factors are determined by performance requirements of microsecond laser cutting machines as shown in Section 3. Table 7 shows the value ranges and the incremental step for these parameters: h is from 2.0 to 3.5 mm, δ is from 1.6 to 2.2 mm, τ is from 17 to 20 mm, and l is from 6.0 to 7.5 mm as the incremental level step of each factor is 0.5 mm, 0.2 mm, 1.0 mm, and 0.5 mm, respectively.

Table 7. Levels of the structural parameters.

Variables	Level 1	Level 2	Level 3	Level 4
h	2.0 mm	2.5 mm	3.0 mm	3.5 mm
δ	1.6 mm	1.8 mm	2.0 mm	2.2 mm
τ	17 mm	18 mm	19 mm	20 mm
l	6.0 mm	6.5 mm	7.0 mm	7.5 mm

According to Table 7, four different factors and four levels of each factor result in $4^4 = 256$ different combinations. All of the 256 groups' data of the performances of PMSLM after the calculation of 3D-FEA is shown in Table 8. The data shown in Table 8 conceal the relationship between the different structural parameters and motor output performance. These data are prepared for following multi-SVM, exploring the relation between input and output variables.

Table 8. Sample data space based on 3D-FEA.

Structure Parameter Variables					Output Performances		
No.	h	δ	τ	l	F (N)	η (%)	THD (%)
1	2.0	1.6	17	6.0	36.084	10.804	5.214
2	2.0	1.6	17	6.5	35.862	10.817	5.127
3	2.0	1.6	17	7.0	36.591	11.207	6.517
4	2.0	1.6	17	7.5	36.289	11.159	6.425
5	2.0	1.6	18	6.0	36.335	10.791	6.333
...	...	...	...	...	...	...	...
...	...	...	...	...	...	...	...
254	3.5	2.2	20	6.5	37.432	9.381	4.89
255	3.5	2.2	20	7.0	39.484	9.385	5.12
256	3.5	2.2	20	7.5	39.118	9.316	5.67

4.2. Multiple SVM for PMSLM

Exploring the objective function—F(x), which can calculate any output value y for any input x, is the essence of SVM [27–31]. The multi-SVM is the modified SVM algorithm, which contains the multidimensional vector output y. All of the structural parameters can be seen as the input parameters compared to all of the performances, which can be seen as the output parameters, by training the input parameters and output performances shown in Table 7. The relations between the multidimensional inputs and outputs are obtained, and the output performances of any other input is subjected to regression calculation using the non-parametric relation between the inputs and outputs of the training data. The core steps of multi-SVM are as follows:

Step 1: Single SVM modeling. By training the input parameters and calculations for the output function F(x), different SVM models (i.e., thrust SVM and THD SVM) are established. The kernel function—$K(x, z)$ of the single SVM model is selected as follows:

$$K(x,z) = \rho_1 (x,z)^d - \rho_2 \|x-y\|^q + 1, \quad \rho_1 + \rho_2 = 1, q = 1, d = 2 \tag{4}$$

where d is the number of dimension, q is constant number, and ρ_1 and ρ_2 are the proportions of different kernels.

Step 2: Fusion of the single SVM models. Following the principle of structure risk minimum, the regression problem is translated into a constrained optimization problem after the best W and B in Equation (5) are searched with the fusion algorithm:

$$\min R(W) = \frac{1}{2}\sum_{i=1}^{N} \|w_i\|^2 + C\sum_{i=1}^{L} Q(h_i), \quad h_i = \|e_i\|, e_i = y_i - (W, \phi(x_i)) + B \tag{5}$$

where N is the dimension number of output performances, C is the penalty parameter, h_i is the empirical error and $\phi(x_i)$ is the nonlinear mapping function.

Aimed at the function fitting problem of N dimension inputs and M dimension outputs, the training sample is set as $\{(x_i, y_i), i = 1, 2, 3 \ldots, L, x_i \in R^N, y_i \in R^M\}$. The multi-SVM objective function F(x) is expressed as follows, where $K(x_i, x)$ is the kernel function, b_i is the constant, and w^j is the regression coefficient:

$$y = f(x) = \sum_{i=1}^{l} (\overline{\partial_i^*} - \overline{\partial}) K(x_i, x) + b \tag{6}$$

$$K(x_i, x) = [\phi(x_i) * \phi(x)], w^j = \sum_{i=1}^{l} (\overline{\partial_i^*} - \overline{\partial}) * \phi(x_i) \tag{7}$$

$$F(x) = \begin{bmatrix} f_1(x) \\ \vdots \\ f_n(x) \end{bmatrix} = \begin{bmatrix} (w_1^1 * \phi_1(x)) + b_1^1 + (w_2^1 * \phi_2(x)) + b_2^1 \\ \vdots \\ (w_1^n * \phi_1(x)) + b_1^n + (w_2^n * \phi_2(x)) + b_2^n \end{bmatrix} = \begin{bmatrix} w_1^1, w_2^1 \\ \vdots \\ w_1^n, w_2^n \end{bmatrix} * \begin{bmatrix} \phi_1(x) \\ \phi_2(x) \end{bmatrix} + B = W * \phi(X) + B, \quad B = [b_1, b_2 \ldots, b_n] \tag{8}$$

After 100 groups of input parameters data are imported to the multi-SVM model, 100 groups of output parameter data predicted by multi-SVM are compared with the original output parameter data. Figure 7 shows that the accuracy of the multi-SVM motor model can reach 95.7% or even more and that the error rate can be limited to 1.2%. After the regression fitting of multi-SVM. The discrete data space by 3D-FEA is translated into a continuous data space, which can provide a quick calculation model for the succeeding GCNA optimization.

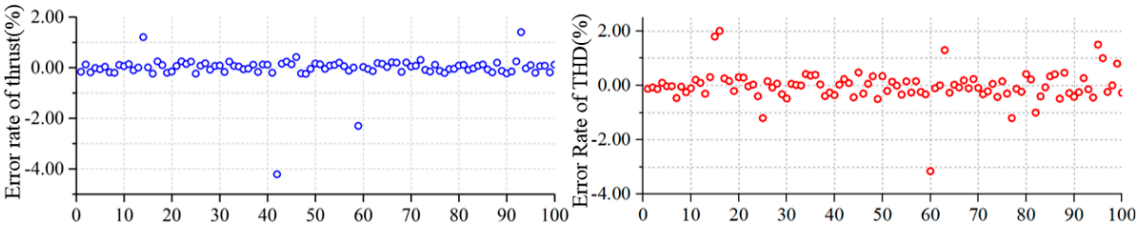

Figure 7. Error rate of multi-SVM: (**a**) error rate of thrust (%); and (**b**) error rate of THD (%).

4.3. Gravity Center Neighborhood Algorithm

Gravity center can be seen as the force balance point that satisfies the "level principle" [14]. The thin plank model-$f(x)$ is shown in Figure 8, where the points B, C, and D are the top of three bulges. The gravity center of the thin plank is determined by the object-hanging method. The gravitational

lines l_a and l_e are obtained by choosing points A and E to hang up the plank, and the intersection O is the gravity center of this plank.

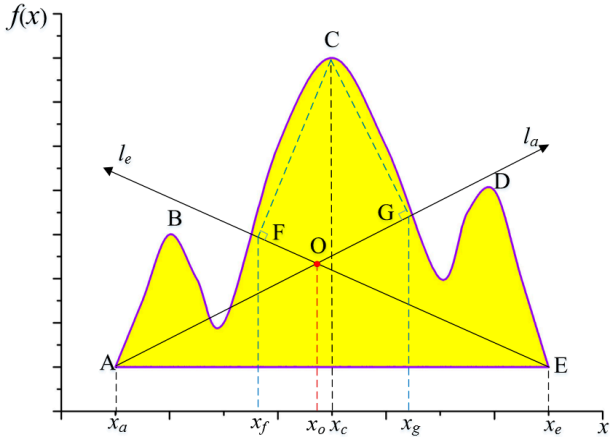

Figure 8. Determination of the gravity center by object-hanging.

Evidently, points B and D are the extrema of $f(x)$, given that point C is the global maximum of $f(x)$. An interesting phenomenon is that the gravity center O is very close to the highest point C along the X-axis. This phenomenon can be explained by the knowledge of the moment equilibrium because the moments on both sides of the gravitational lines are equal. C must lie on the left by l_a and on the right by l_e, which can result in the location of the intersection O at the very close neighborhood of C along the X-axis. Assuming that the plank model $f(x)$ can be expressed by the equations as $f(x)$, the optimization problem is to find the global maximum of $f(x)$. The two gravitational lines are determined by the location of the gravity center. CF and CG are the shortest distances from C to l_a and l_e. The neighborhood area of the global maximum can be expressed as [min (x_f, x_g), max (x_f, x_g)], and the neighborhood area decreases gradually by several times of the iterative computations. The global maximum is then obtained easily using the gravity center location method.

To avoid premature convergence and a local optimum, the GCNA is introduced. Its operating steps, as shown in Figure 9, are as follows.

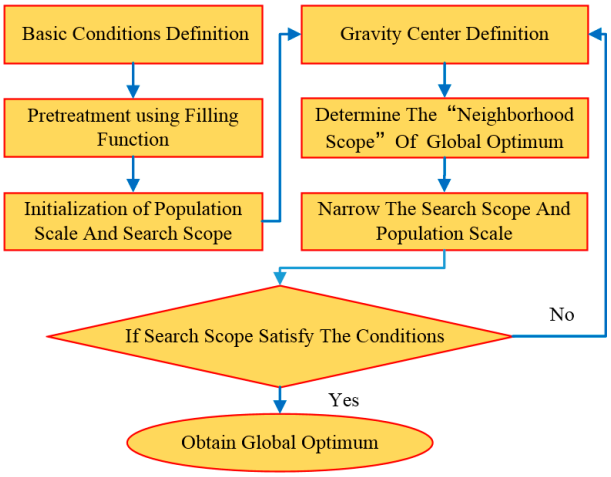

Figure 9. Flowchart of the GCNA.

Step 1—Basic Conditions Definition

Confirm the objective function and optimize the variables and the range of parameters.

Step 2—Pretreament using a Filling Function

Select the "filling function" [32,33] shown in Equation (8) to promote the accuracy of the gravity center location and to avoid the local optimum:

$$p(x, x^*) = -\phi[f(x) - f(x^*) + \alpha] \times \|x - x^*\|^2 \tag{9}$$

where x^* is the current local extreme point, α is the parameter named "filling factor", which influences the filling effect largely, and ϕ(t) satisfies the following conditions:

(1) $\phi(0) > 0$;
(2) ϕ(t) is derivable and $t \neq 0$, $\phi'(t) > 0$

Step 3—Initialization of Population Scale and Search Scope

Initialize the search scope $\Omega(0)$, which is determined by the variable ranges; the initialized population scale $P(0)$ is determined by considering convergence rate and optimizing accuracy.

Step 4—Gravity Center Definition

The gravity center location of the objective function is determined via the following search strategy:

$$x_o(k) = \frac{F(x_b)x_b + \sum_{i=2}^{P(k)} F(x_i(k))x_i(k)}{F(x_b) + \sum_{i=2}^{P(k)} F(x_i(k))} \tag{10}$$

where F(x_b) is optimal of the before $k-1$ times iterations. This strategy can lead to movement of the "gravity center" along the direction of the global optimum effectively.

Step 5—Determine the "Neighborhood Scope" of Global Optimum

The neighborhood scope of the gravity center can be expressed by the follow equation:

$$\Omega_0 = \Omega(0)\eta^d / N \tag{11}$$

where η ($\eta < 1$) is the scope compression rate, d is the dimension of the optimizing scope, and N is the search times

Step 6—Narrow the Search Scope and Population Scale

(1) The kth search scope can be expressed as follows:

$$\Omega(k) / \Omega(k-1) = \eta^d \tag{12}$$

(2) The kth population scope is expressed as follows:

$$\begin{aligned} &P(k) = P(k-1)e^{\gamma(\eta^d - 1)\eta^d / (k-N-1)}, k \leq N \\ &\gamma = \rho\eta^d / d \end{aligned} \tag{13}$$

where ρ is an adjustable parameter.

Step 7—Condition of Convergence

$$\Omega(k) = \Omega_0 \tag{14}$$

When Equation (13) is set up, the search scope is equal to the neighborhood scope of the gravity center. The current gravity center can be seen as the global optimum. Otherwise, return to Step 4.

4.4. Optimization of PMSLM

This study adopts the GCNA to optimize the multi-SVM motor model. The parameters of the GCNA are shown in Table 9, where $P(0)$ is initialized population scale, $\Omega(0)$ is the search scope, d is the dimension of the optimizing scope, η is the scope compression rate, N is the search times, α is the parameter named "filling factor", and ρ is an adjustable parameter. The evolutionary process diagrams of the GCNA are shown in Figure 10.

Table 9. Parameters of GCNA.

$P(0)$	$\Omega(0)$	d	η	N	α	ρ
768	3^4	4	0.45	250	0.0001	0.02

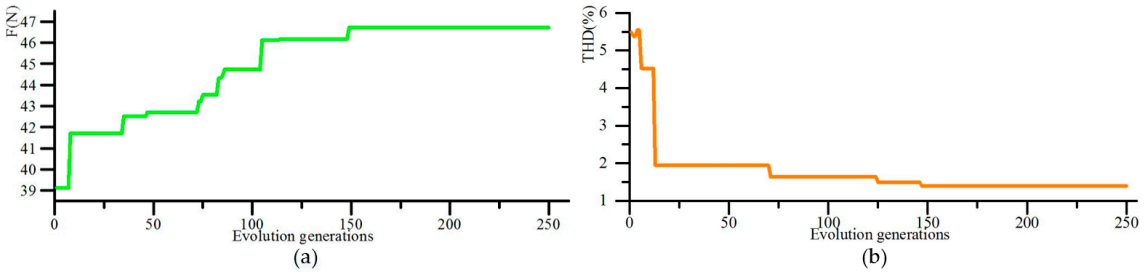

Figure 10. Evolutionary process diagrams: (**a**) Evolution progress of thrust; and (**b**) Evolution progress of THD.

The global optimal combination of the PMSLM structure parameters is obtained after the iteration calculations of GCNA. Table 10 shows the comparison of the structural parameters of the Taguchi method, new method, and experimental method clearly.

Table 10. Comparison of structural parameters.

Parameters	Taguchi	New	Experimental
h	2.75 mm	3.05 mm	3.05 mm
δ	1.90 mm	2.09 mm	2.09 mm
τ	20.00 mm	19.12 mm	19.12 mm
l	6.75 mm	6.57 mm	6.57 mm

5. Experimental Verification

To validate the performances of optimized PMSLM, a prototype of PMSLM is manufactured and the test platform is established as shown in Figure 11.

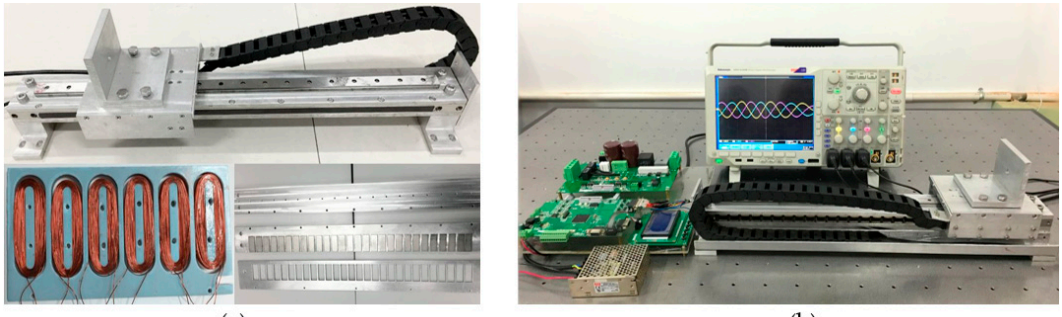

Figure 11. Test platform for the manufactured PMSLM: (**a**) Prototype of PMSLM; and (**b**) Test platform.

In Figure 12, the no-load inductive electromotive force (EMF) lines and harmonic analysis of the Taguchi method, new method, and experimental method are respectively shown.

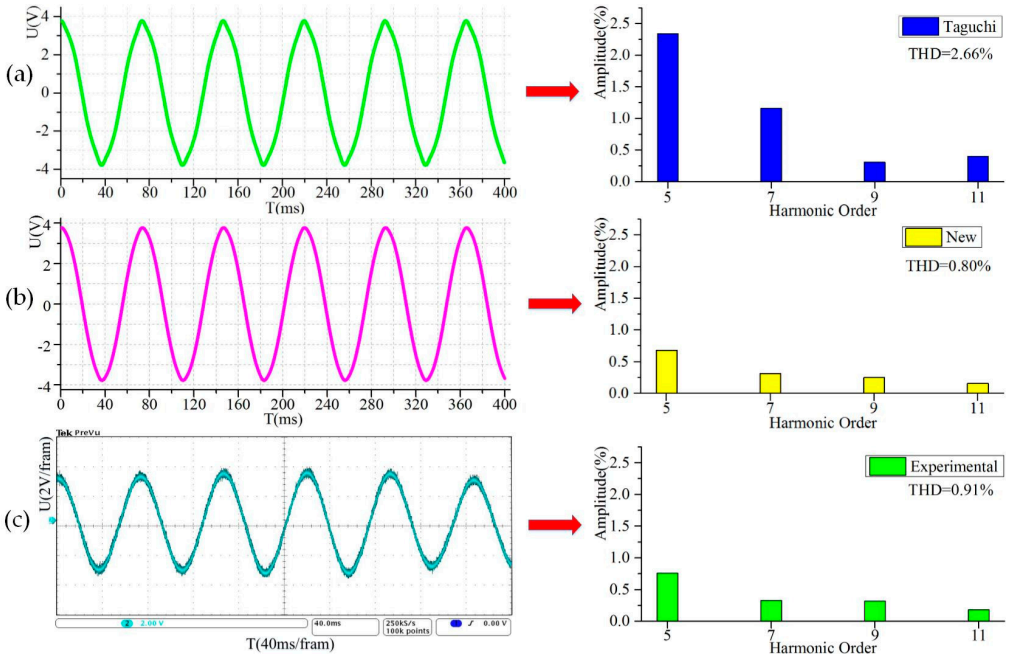

Figure 12. Inductive EMF and harmonic analysis by three methods: (**a**) Taguchi; (**b**) New; and (**c**) Experimental.

The sinusoidal characteristic of the new method is evidently promoted relative to the Taguchi method. The comparative results of the harmonic amplitude after spectrum analysis [34,35] are shown in Figure 12 and Table 11. Due to the star connection of coils, there is no 3rd harmonic. The experimental results show that the harmonics of the 5th, 7th, 9th, and 11th are restrained by 0.76%, 0.33%, 0.32%, and 0.18%, respectively, which indicates that the harmonic content significantly decreases. The THD of the Taguchi method, new method, and experimental results are 2.66%, 0.80%, and 0.91%. The THD of experimental results are remarkably reduced 69.92% compared with the Taguchi method. Given the decrease in harmonic content and improvement in THD, the stability of PMSLM can be enhanced significantly.

Table 11. Comparison of harmonic content.

Amplitude%	Harmonic Order					THD%
	1st	5th	7th	9th	11th	
Taguchi	100%	2.34%	1.16%	0.31%	0.40%	2.66%
New	100%	0.68%	0.31%	0.25%	0.16%	0.80%
Experimental	100%	0.76%	0.33%	0.32%	0.18%	0.91%

As shown in Table 12 and Figure 13, the thrust experimental results indicate that the motor average thrust reaches 43.713 N and the thrust ripple is suppressed to 1.969%, which represents an enhancement of the Taguchi method.

Table 12. Comparison of thrust.

	Taguchi	New	Experimental
F (N)	40.241	43.713	43.279
η (%)	6.342%	1.937%	1.969%

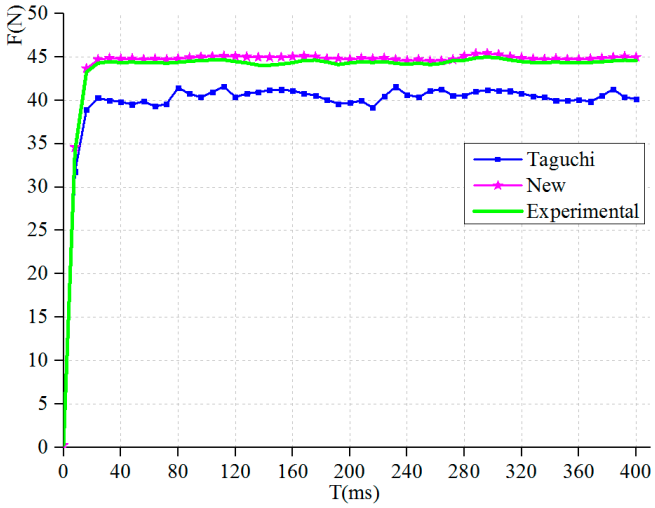

Figure 13. Comparison of motor thrust.

All the performances of PMSLM are influenced by the motor structure parameters. From Taguchi to the new method, the volume of the magnets increases by 10.9%, owing to the increase in magnet height which can enhance the magnetic field intensity. The thrust curve of the new method is more stable because of the lowest thrust ripple, which is mainly affected by the air gap and pole pitch when the motor mover passes by different adjacent magnets. The combination of a 2.09 mm air gap and 19.12 mm pole pitch is the most suitable for magnetic distribution. A 1.937% thrust ripple can guarantee the placid operation of the mover. All of these findings indicate the validity of the proposed new method.

6. Conclusions

The PMSLM applied in microsecond laser cutting machines with no cutting force is presented in this paper. A new optimization method is introduced to the motor design optimization. Through the 3D-FEM analysis of PMSLM performance, multi-SVM is proposed to develop the mapping relation from multivariate structure parameters to multivariate operational performances, which can result in the formation of a non-parametric quick calculation model. After the optimization iteration calculations of the GCNA, the global optimal combination of motor structure parameters, such as the height of magnet, air gap, pole pitch, and coil length, are obtained by the gravity center location of the objective function. Through the analysis of harmonic content, the THD %, thrust, thrust ripple, and operational performances of PMSLM are enhanced remarkably. This method is verified by an experimental test, and the design goals and optimization results have a great consistency.

7. Discussion

In the future work, the authors will continue to research the following directions to enhance this optimization method:

(1) Enlarge the value range of the design parameters. In the larger value ranges, attempt to find more suitable combinations of design parameters which can satisfy the requirements of microsecond laser cutting machines. Namely, thrust should be no less than 35 N, and thrust ripple and harmonic contents should be the lowest.

(2) Research more design parameters (such as 10–15 parameters) to certify this method. On the basis of four parameters shown in Table 1, more design parameters will be investigated to verify the effectiveness of the proposed new optimization method. The additional parameters include the width of magnets, the length of magnets, the thickness of back-iron, the structure of coils, and so on.

(3) Promote the computational efficiency. The authors will reduce the unnecessary finite-element meshing in FEM software, ANSOFT (ANSYS, Pittsburgh, PA, USA), and to study new software, INFOLYTICA (INFOLYTICA, Montreal, Quebec, Canada) which can reduce the computing time by at least about 35%.

Acknowledgments: This work is supported by the National Natural Science Foundation of China under Grant Nos. 51277002, 51577001 and 51637001. The authors would like to thank the anonymous reviewers for their valuable comments and suggestions.

Author Contributions: All authors contributed to this work by cooperation. Juncai Song, Fei Dong, Le Li and Zhenbao Pan are the main authors of this manuscript and this work was conducted under the advisement of Jiwen Zhao and Siliang Lu.

Conflicts of Interest: The authors declare no conflict of interest.

References

1. Li, L.; Tang, Y.; Pan, D. Design optimization of air-cored PMLSM with overlapping windings by multiple population genetic algorithm. *IEEE Trans. Magn.* **2014**, *50*, 1–5. [CrossRef]
2. Cai, J.J.; Lu, Q.; Huang, X.; Ye, Y. Thrust ripple of a permanent magnet LSM with step skewed magnets. *IEEE Trans. Magn.* **2012**, *48*, 4666–4669. [CrossRef]
3. Zhu, Y.W.; Lee, S.G.; Chung, K.S.; Cho, Y.H. Investigation of auxiliary poles design criteria on reduction of end effect of detent force for PMLSM. *IEEE Trans. Magn.* **2009**, *45*, 2863–2866. [CrossRef]
4. Duan, Y.; Ionel, D.M. A review of recent developments in electrical machine design optimization methods with a permanent-magnet synchronous motor benchmark study. *IEEE Trans. Ind. Appl.* **2013**, *49*, 1268–1275. [CrossRef]
5. Pfister, P.D.; Perriard, Y. Very-high-speed slotless permanent-magnet motors: Analytical modeling, optimization, design, and torque measurement methods. *IEEE Trans. Ind. Electron.* **2010**, *57*, 296–303. [CrossRef]
6. Siadatan, A.; Afjei, E.; Torkaman, H. Analytical design and fem verification of a novel three-phase seven layers switched reluctance motor. *Prog. Electromagn. Res.* **2013**, *140*, 131–146. [CrossRef]
7. Hasanien, H.M.; Abd-Rabou, A.S.; Sakr, S.M. Design optimization of transverse flux linear motor for weight reduction and performance improvement using response surface methodology and genetic algorithms. *IEEE Trans. Energy Convers.* **2010**, *25*, 598–605. [CrossRef]
8. Lebensztajn, L.; Costa, M.C.; Coulomb, J.L. Kriging: A useful tool for electromagnetic device optimization. *IEEE Trans. Megn.* **2004**, *40*, 1196–1199. [CrossRef]
9. Lei, G.; Guo, Y.G.; Zhu, J.G.; Chen, X.M.; Xu, W.; Shao, K.R. Sequential subspace optimization method for electromagnetic devices design with orthogonal design technique. *IEEE Trans. Magn.* **2012**, *48*, 479–482. [CrossRef]
10. Hwang, C.C.; Lyu, L.Y.; Liu, C.T.; Li, P.L. Optimal design of an spm motor using genetic algorithms and Taguchi method. *IEEE Trans. Magn.* **2008**, *44*, 4325–4328. [CrossRef]
11. Lei, G.; Wang, T.; Zhu, J.; Guo, Y.; Wang, S. System-level design optimization method for electrical drive systems—Robust approach. *IEEE Trans. Ind. Electron.* **2015**, *62*, 4702–4713. [CrossRef]
12. Lei, G.; Wang, T.; Guo, Y.; Zhu, J.; Wang, S. System-level design optimization methods for electrical drive systems: Deterministic approach. *IEEE Trans. Ind. Electron.* **2014**, *61*, 6591–6602. [CrossRef]
13. Lei, G.; Zhu, J.G.; Guo, Y.G.; Hu, J.F.; Xu, W.; Shao, K.R. Robust design optimization of PM-SMC motors for six sigma quality manufacturing. *IEEE Trans. Magn.* **2013**, *49*, 3953–3956. [CrossRef]
14. Lei, G.; Liu, C.; Zhu, J.; Guo, Y. Techniques for multilevel design optimization of permanent magnet motors. *IEEE Trans. Energy Convers.* **2015**, *30*, 1574–1584. [CrossRef]
15. Wang, M.H.; Huang, M.L.; Zhan, Z.Y.; Huang, C.J. Application of the extension Taguchi method to optimal capability planning of a stand-alone power system. *Energies* **2016**, *9*. [CrossRef]
16. Hsiao, C.Y.; Yeh, S.N.; Hwang, J.C. Design of high performance permanent-magnet synchronous wind generators. *Energies* **2014**, *7*, 7105–7124. [CrossRef]
17. Omekanda, A.M. Robust torque and torque-per-inertia optimization of a switched reluctance motor using the Taguchi methods. *IEEE Trans. Ind. Appl.* **2005**, *42*, 473–478. [CrossRef]
18. Lee, S.; Kim, K.; Cho, S.; Jang, J. Optimal design of interior permanent magnet synchronous motor considering the manufacturing tolerances using Taguchi robust design. *IET Electr. Power Appl.* **2014**, *8*, 23–28. [CrossRef]

19. Hasanien, H.M. Particle swarm design optimization of transverse flux linear motor for weight reduction and improvement of thrust force. *IEEE Trans. Ind. Electron.* **2011**, *58*, 4048–4056. [CrossRef]
20. Bernieri, A.; Betta, G.; Ferrigno, L.; Laracca, M. Multifrequency excitation and support vector machine regressor for ECT defect characterization. *IEEE Trans. Instrum. Meas.* **2014**, *63*, 1272–1280. [CrossRef]
21. Soualhi, A.; Medjaher, K.; Zerhouni, N. Bearing health monitoring based on hilbert-huang transform, support vector machine, and regression. *IEEE Trans. Instrum. Meas.* **2015**, *64*, 52–62. [CrossRef]
22. Liu, Y.H.; Huang, H.P.; Weng, C.H. Recognition of electromyographic signals using cascaded kernel learning machine. *IEEE Trans. Mech.* **2007**, *12*, 253–264. [CrossRef]
23. Yang, Q.; Liu, Y.; Wang, S.; Xue, Y. A method to locate neighborhood of global optimum. In Proceedings of the International Conference on Natural Computation, Chongqing, China, 29–31 May 2012.
24. Cao, W.; Tian, Z.Y.; Qiao, H.D. A new filled function method applied to unconstrained global optimization. *J. Qingdao Univ.* **2008**, *225*, 501–512.
25. Sarikhani, A.; Mohammed, O.A. HIL-based finite-element design optimization process for the computational prototyping of electric motor drives. *IEEE Trans. Energy Convers.* **2012**, *27*, 737–746. [CrossRef]
26. Tsili, M.A.; Amoiralis, E.I.; Kladas, A.G.; Souflaris, A.T. Optimal design of multi-winding transformer using combined FEM, taguchi and stochastic-deterministic approach. *IET Electr. Power Appl.* **2012**, *6*, 437–454. [CrossRef]
27. Del Valle, Y.; Venayagamoorthy, G.K.; Mohagheghi, S.; Hernandez, J.C.; Harley, R.G. Particle swarm optimization: Basic concepts, variants and applications in power systems. *IEEE Trans. Evol. Comput.* **2008**, *12*, 171–195. [CrossRef]
28. Gao, R.; Ye, S. Improved adaptive pruning algorithm for least squares support vector regression. *J. Syst. Eng. Electron.* **2012**, *23*, 438–444. [CrossRef]
29. Sanchez-Fernandez, M.; De-Prado-Cumplido, M.; Arenas-Garcia, J.; Perez-Cruz, F. SVM multiregression for nonlinear channel estimation in multiple-input multiple-output systems. *IEEE Trans. Signal. Process.* **2004**, *52*, 2298–2307. [CrossRef]
30. Lin, W.J.; Jhuo, S.S. A fast luminance inspector for backlight modules based on multiple kernel support vector regression. *IEEE Trans. Compon. Packag. Manuf. Technol.* **2014**, *4*, 1391–1401.
31. Huang, S.; Cao, G.; He, Z.; Pan, J.F. Nonlinear modeling of the inverse force function for the planar switched reluctance motor using sparse least squares support vector machines. *IEEE Trans. Ind. Inf.* **2015**, *11*, 591–600. [CrossRef]
32. Liu, X. A class of continuously differentiable filled functions for global optimization. *IEEE Trans. Syst. Man Cybern.* **2008**, *38*, 38–47.
33. Liu, J.; Ye, Z.Q. A new class of filled functions for finding global optimization. *Comput. Technol. Dev.* **2010**, *20*, 36–38.
34. Chattopadhyay, S.; Chattopadhyaya, A.; Sengupta, S. Analysis of stator current of induction motor used in transport system at single phasing by measuring phase angle, symmetrical components, skewness, kurtosis and harmonic distortion in park plane. *IET Electr. Syst. Transp.* **2013**, *4*, 1–8. [CrossRef]
35. Zhang, Y.J.; Zha, F.T.; Ling, J.; Wan, T. Low RCS dipole array synthesis based on MoM-PSO hybrid algorithm. *Prog. Electromagn. Res.* **2009**, *94*, 119–132. [CrossRef]